Computational Materials Science 48 (2010) 213–227

Contents lists available at ScienceDirect

Computational Materials Science

journal homepage: www.elsevier.com/locate/commatsci

Microstructure model reduction and uncertainty quantification in multiscale deformation processes

Babak Kouchmeshky, Nicholas Zabaras *

Materials Process Design and Control Laboratory, Sibley School of Mechanical and Aerospace Engineering, 101 Frank H.T. Rhodes Hall, Cornell University, Ithaca, NY 14853-3801, USA

ARTICLE INFO

Article history:
Received 1 September 2009
Received in revised form 3 December 2009
Accepted 3 January 2010
Available online 29 January 2010

Keywords:
Multiscale modeling
Polycrystal plasticity
Processing
Texture
Mechanical properties
Probability and statistics
Uncertainty quantification

ABSTRACT

The quantification and propagation of uncertainty in multiscale deformation processes is considered. A reduced-order model for representing the data-driven stochastic microstructure input is presented. The multiscale random field representing the random microstructure is decomposed into few modes in different scales (the Rodrigues space for representing texture on mesoscale and the continuum macroscale space). Realizations from a stochastic simulation are used to obtain a small number of modes approximating the stochastic field. An example of a multiscale closed-die forging problem is provided in which the effects of uncertain initial geometry and texture on the macroscale properties are studied.

1. Introduction

Macroscale properties of polycrystalline alloys depend on the preferred orientation of crystals in the underlying microstructure manifested as the crystallographic texture. During deformation processes, mechanisms such as crystallographic slip and lattice rotation drive the formation of texture. Variability in such processes and uncertainty in the initial texture of the material subjected to these processes have a significant effect on the final macroscale properties. Obtaining the variation in material properties due to the inherent randomness of the microstructure is an important component in any materials design. This leads one to use stochastic methods in calculating the effect of uncertainties in initial texture and geometry on the final macroscale properties of the workpiece.

The multiscale phenomena of crystal re-orientation in a deformation process using finite element discretization have been the topic of previous works [1–3]. In [1], a multiscale sensitivity framework for the control of macroscale properties in deformation processing has been studied. Acharjee and Zabaras [4] have studied the effect of uncertain initial geometry for a deformation processing problem using a phenomenological constitutive model.

On the propagation of uncertainty area, there has been significant progress in posing and solving stochastic partial differential equations [5–7]. Model reduction approaches for stochastic systems have also emerged in recent works [8–11]. The effects of uncertain initial texture and processing parameters on the convex hull of macroscale properties were studied recently in [12] using a point simulator. The effect of uncertain material properties in a multiscale diffusion problem is presented in [13]. The reduced-order model considered was only implemented on the mesoscale. The method presented in [13] is viable for cases where the correlation length of material properties is much smaller than the shortest distance between the integration points on the macroscale. For the problems where there is a much larger correlation length for material properties, this method will result in a number of independent random variables at each integration point on the macroscale. This high-stochastic dimensionality in turn leaves no choice in [13] but to use Monte-Carlo techniques to analyze the multiscale diffusion problem that they examined.

Including the underlying microstructure and its evolution for every integration point on the macroscale is essential in quantifying the effect of a deformation process on the macroscale properties. This paper provides the first steps towards developing a rigorous methodology for addressing this problem using a bi-orthogonal model [9] to describe the variability of the initial microstructure. The random field describing the system input (the initial microstructure) is decomposed into modes in two different scales, the Rodrigues space and the continuum spatial domain. The

* Corresponding author. Fax: +1 607 255 1222.
E-mail address: zabaras@cornell.edu (N. Zabaras).
URL: http://mpdc.mae.cornell.edu/ (N. Zabaras).

0927-0256/$ - see front matter © 2010 Elsevier B.V. All rights reserved.
doi:10.1016/j.commatsci.2010.01.001

coefficients of the polynomial chaos terms in this expansion are obtained using projections of the random modes on the chaos polynomials. For propagating the uncertainty, a sparse grid collocation strategy [7] is considered that utilizes the deterministic multiscale deformation simulator.

As the number of random variables increases, the computational effort needed to solve a stochastic multiscale deformation problem rapidly becomes a burden. The aim of this paper is to present a general data-driven framework for model reduction of the input microstructure uncertainty that arises. This framework is meant to eliminate the need for redundant correlated random variables that would be needed in case of using methods as in [13]. Hence it can be used to quantify the effects of uncertainty in the multiscale problem under study.

The plan of this paper is as follows. Section 2 provides some background on the constitutive polycrystal plasticity model, texture evolution and kinematics in the multiscale deformation problem. Section 3 provides the problem definition. Section 4 briefly reviews the sparse grid collocation method used in solving the stochastic differential equations. The reduced-order model is presented in Section 5 and summary of the polynomial chaos expansion used in the reduced-order model is presented in Section 6. Finally, Sections 7 and 8 present the numerical examples and conclusions, respectively.

2. Constitutive problem and texture evolution

During a deformation process, crystallographic slip and re-orientation of crystals (lattice rotation) can be assumed to be the primary mechanisms of plastic deformation. The slip and re-orientation occur in an ordered manner such that a preferential orientation or texture develops. We follow the rate-independent constitutive model developed in [14].

Consider a particular crystal orientation, in an appropriate kinematic framework the total deformation gradient is decomposed into plastic and elastic parts $\boldsymbol{F} = \boldsymbol{F}^e\boldsymbol{F}^p$, where $\boldsymbol{F}^e$ is the elastic deformation gradient and $\boldsymbol{F}^p$, the plastic deformation gradient, with $\det \boldsymbol{F}^p = 1$. The constitutive relation is given by

$$\overline{\boldsymbol{T}} = \mathscr{L}^e[\overline{\boldsymbol{E}}^e] \tag{1}$$

where $\overline{\boldsymbol{T}}$ is the second Piola–Kirchhoff stress tensor, $\mathscr{L}^e$ is the fourth-order anisotropic elasticity tensor expressed in terms of the crystal stiffness parameters and the orientation $\boldsymbol{r}$ and $\overline{\boldsymbol{E}}^e = \frac{1}{2}(\boldsymbol{F}^{eT}\boldsymbol{F}^e - \boldsymbol{I})$. The re-orientation velocity is found as follows:

$$\boldsymbol{v} = \frac{\partial \boldsymbol{r}}{\partial t} = \frac{1}{2}(\boldsymbol{\varpi} + (\boldsymbol{\varpi}\cdot\boldsymbol{r})\boldsymbol{r} + \boldsymbol{\varpi}\times\boldsymbol{r}) \tag{2}$$

where $\boldsymbol{r}$ is the orientation (Rodrigues' parameterization) and $\boldsymbol{\varpi}$ represents the spin vector defined as $\boldsymbol{\varpi} = \mathrm{vect}(\dot{\boldsymbol{R}}^e\boldsymbol{R}^{eT})$, where $\boldsymbol{R}^e$ is evaluated through the polar decomposition of the elastic deformation gradient $\boldsymbol{F}^e$ as $\boldsymbol{F}^e = \boldsymbol{R}^e\boldsymbol{U}^e$.

Consider a macroscopic material point and an associated underlying microstructure $\mathscr{M}$ discretized by a grid (Fig. 1). Each point on this underlying grid corresponds to a different crystal orientation $\boldsymbol{R}$. At each point on the grid, the crystal lattice frame $\hat{\boldsymbol{e}}_i$ is related to the sample reference frame $\boldsymbol{e}_i$ by $\boldsymbol{e}_i = \boldsymbol{R}\hat{\boldsymbol{e}}_i$.

The Rodrigues–Frank axis-angle parameterization is used as a convenient scheme to represent $\boldsymbol{R}$ [15]. The parameterization is derived from the natural invariants of $\boldsymbol{R}$: the axis of rotation $\boldsymbol{n}$ and the angle of rotation $\hat{\zeta}$. The angle-axis parameterization, $\boldsymbol{r}$, is obtained by scaling the axis $\boldsymbol{n}$ by a function of the angle $\hat{\zeta}$ as $\boldsymbol{r} = \boldsymbol{n}f(\hat{\zeta})$. In the particular case of Rodrigues' parameterization, the function is defined as $f(\hat{\zeta}) = \tan\left(\frac{\hat{\zeta}}{2}\right)$. Due to crystal symmetry, the Rodriguez parameterization of orientation is not unique. Restricting the Rodriguez domain to a fundamental zone that reflects the crystal symmetry leads to a one-to-one correspondence between the points on the Rodriguez space and the crystal orientation.

To represent a particular texture, an orientation distribution function $A(\boldsymbol{r})$ is defined on a three-dimensional bounded domain $\mathscr{R}$ called Rodrigues space that describes the crystal density over the fundamental region [16–18]. Through such a description, the microstructure is treated as a continuum of crystals. The representation of the orientation distribution function (ODF) in an Eulerian framework is $A(\boldsymbol{r}, t)$, whereas in a Lagrangian framework is given as $\widehat{A}(s,t)$, where $A(\boldsymbol{r},t) = A(\hat{\boldsymbol{r}}(s,t),t) = \widehat{A}(s,t)$, with $\hat{\boldsymbol{r}}$ the re-orientation vector.

For cubic symmetry, the fundamental zone is shown in Fig. 2a. It can be shown [19] that each symmetry rotation $\hat{\zeta}$ along axis $\boldsymbol{n}$ translates to a pair of planes in Rodrigues space with normals $\pm\boldsymbol{n}$ at a distance equal to $\tan\left(\frac{\hat{\zeta}}{4}\right)$ from the origin. The inner envelope of the planes created due to symmetry is the fundamental zone. For example in the cubic symmetry case, the faces of the fundamental zone are due to symmetry rotations about $\langle 100\rangle$ family of axes and their distance to the origin is $\tan(\pi/8)$. The corners of the fundamental zone are due to the planes created by the symmetry rotations along $\langle 111\rangle$ axes and their distance to the origin is $\tan(\pi/6)$ [19].

Orientations on each parallel pair of planes that form the faces and corners of the fundamental zone are equivalent under the symmetries. In the cubic fundamental region, orientations on the parallel pairs of $\{100\}$ faces are equivalent by an offset. This offset is determined by rotation of $\pi/4$ about the corresponding $\langle 100\rangle$ axes. The same equivalence holds for $\{111\}$ faces where the offset is a rotation of $\pi/3$ about the corresponding $\langle 111\rangle$ axes [19].

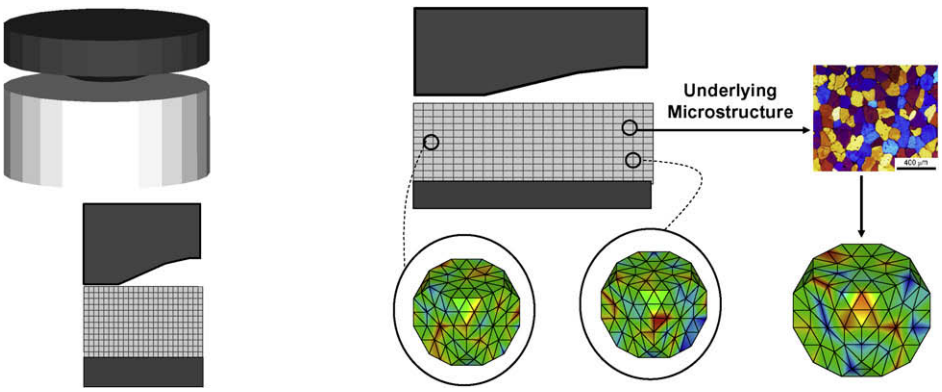

Fig. 1. (Left) Schematic view of the workpiece and die in a forging process. (Right) schematic view of the multiscale problem.

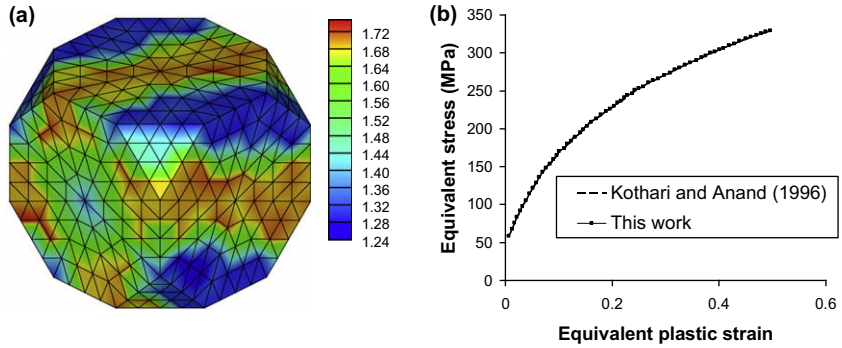

Fig. 2. (a) Texture obtained for an FCC copper polycrystal subjected to a simple compression mode is shown over the fundamental part of Rodrigues space. (b) Comparison of the equivalent stress–strain response with results from [14].

The Lagrangian scheme for the ODF evolution as described in [16] is used. The evolution of the ODF is governed by the ODF conservation equation and is given in the Lagrangian form as follows:

$$\frac{\partial \widehat{A}(s,t)}{\partial t} + \widehat{A}(s,t) \bigtriangledown \cdot \boldsymbol{v}(s,t) = 0 \tag{3}$$

where $\boldsymbol{v}(s,t)$ is the Lagrangian re-orientation velocity of the crystals and the Lagrangian form of the ODF, $\widehat{A}(s)$, is subjected to $\widehat{A}(s,0) = \widehat{A}_0(s)$ as the initial condition.

Texture evolution is modeled using the above equation. The texture is represented by the ODF on a grid representing the discretized fundamental region of the Rodrigues' parameter space. For the evolution of texture, the conservation equation for the ODF is solved using the finite element method. The constitutive model is solved at each integration point of this grid which represents an orientation and is connected to the macroscale through the Taylor hypothesis. The response of the underlying microstructure is calculated using the polycrystal plasticity model.

Fig. 2 shows an example of the evolved texture for a Copper polycrystal subjected to a simple compression mode. The texture is provided in the form of orientation distribution function and is plotted over the fundamental part of Rodrigues space for FCC crystal structures. The corresponding stress–strain response is also provided in this figure.

The polycrystal average of an orientation dependent property, $X(s,t)$, is determined as:

$$\langle X \rangle = \frac{\int_{\mathscr{R}} X(s)\widehat{A}(s)dv}{\int_{\mathscr{R}} \widehat{A}(s)dv} \tag{4}$$

Here, $dv = (\det g)^{0.5} ds_1 ds_2 ds_3$. Since the orientation space is non-Euclidean, the volume element is scaled by the term $(\det g)^{0.5}$, where g is the metric for the space.

2.1. Kinematics

Consider a deformation process such as a closed-die forging problem. This deterministic multiscale problem consists of the following: the time history of the deformation including the elastic and plastic part, material state and texture are calculated incrementally as the result of external forces and the effect of contact between the workpiece and the die. For this purpose, the deformation problem is divided into kinematic, contact, constitutive and texture evolution subproblems. An updated Lagrangian framework in which the configuration at the previous step B_n is considered as the reference configuration for calculating the material configuration B_{n+1} is used to solve the deformation problem.

Let $\boldsymbol{X}$ be a material particle in $\boldsymbol{B}_0$ and let $\boldsymbol{x} = \tilde{\boldsymbol{x}}(\boldsymbol{X}, t_{n+1})$ be its location at time t_{n+1}. The total deformation gradient can be defined as

$$\boldsymbol{F}(\boldsymbol{X}, t_{n+1}) = \nabla_0 \tilde{\boldsymbol{x}}(\boldsymbol{X}, t_{n+1}) = \frac{\partial \tilde{\boldsymbol{x}}(\boldsymbol{X}, t_{n+1})}{\partial \boldsymbol{X}} \tag{5}$$

Using an updated Lagrangian framework, the total deformation gradient $\boldsymbol{F}$ at time $t = t_{n+1}$ can be expressed in terms of $\boldsymbol{F}_n$ at time $t = t_n$ as follows:

$$\boldsymbol{F} = \boldsymbol{F}_r \boldsymbol{F}_n \tag{6}$$

where $\boldsymbol{F}_r$ is the relative deformation gradient. The equilibrium equation at $t = t_{n+1}$ can be expressed in the reference configuration $\boldsymbol{B}_n$ as,

$$\nabla_n \cdot \langle \boldsymbol{P}_r \rangle + \boldsymbol{f}_r = 0 \tag{7}$$

where ∇_n denotes the divergence in $\boldsymbol{B}_n$. $\boldsymbol{f}_r$ can be represented as

$$\boldsymbol{f}_r = \det \boldsymbol{F}_r \boldsymbol{b} \tag{8}$$

where $\boldsymbol{b}$ is the body force defined on the current configuration $\boldsymbol{B}_{n+1}$. The homogenized Piola–Kirchhoff I stress $\langle \boldsymbol{P}_r \rangle$ is expressed per unit area of $\boldsymbol{B}_n$ and given as follows:

$$\begin{aligned} \langle \boldsymbol{P}_r \rangle &= \langle \det \boldsymbol{F}_r \boldsymbol{T} \boldsymbol{F}_r^{-T} \rangle \\ &= \det \boldsymbol{F}_r \langle \boldsymbol{T} \rangle \boldsymbol{F}_r^{-T} \end{aligned} \tag{9}$$

where $\boldsymbol{T}$ is the Cauchy stress. The Taylor hypothesis for the macro-meso linking is assumed. An incremental quasi-static problem should be solved to determine the displacement field that satisfies Eq. (7). The solution of the deformation problem proceeds incrementally in time starting from the initial configuration $\boldsymbol{B}_0$.

Eq. (7) describes the equilibrium of the body at time t_{n+1} expressed in the updated reference configuration B_n. The incremental quasi-static boundary value problem at time $t = t_{n+1}$ is to find the incremental (with respect to the configuration B_n) displacement field $\boldsymbol{u}(\boldsymbol{x}_n, t_{n+1}) = \boldsymbol{u}_{n+1}$ that will satisfy Eq. (7). The weak form of this equation can be presented as $\widetilde{G}(\boldsymbol{u}_{n+1}, \tilde{\boldsymbol{\eta}}) = 0$, where $\tilde{\boldsymbol{\eta}}$ is a test vector field compatible with the kinematic boundary conditions. To solve this non-linear equation for $\boldsymbol{u}(\boldsymbol{x}_n; t_{n+1})$, a Newton–Raphson iterative scheme along with a line search method is used. Let $\boldsymbol{u}_{n+1}^{k+1}$ and $\boldsymbol{u}_{n+1}^{k}$ be the displacement fields at the end of the $(k+1)$th step and the kth step, respectively, during the Newton–Raphson iterative process. Then, the linearized form of the equation is as follows:

$$\widetilde{G}(\boldsymbol{u}_{n+1}^{k}, \tilde{\boldsymbol{\eta}}) + \frac{\partial \widetilde{G}}{\partial \boldsymbol{u}_{n+1}^{k}} (\boldsymbol{u}_{n+1}^{k+1} - \boldsymbol{u}_{n+1}^{k}) = 0 \tag{10}$$

The linearization of the part of $\widetilde{G}$ which corresponds to the internal work is provided as

$$d\widetilde{G}_{internal} = \int_{\boldsymbol{B}_n} d\langle \boldsymbol{P}_r \rangle \cdot \frac{\partial \tilde{\boldsymbol{\eta}}}{\partial \boldsymbol{x}_n} dV \tag{11}$$

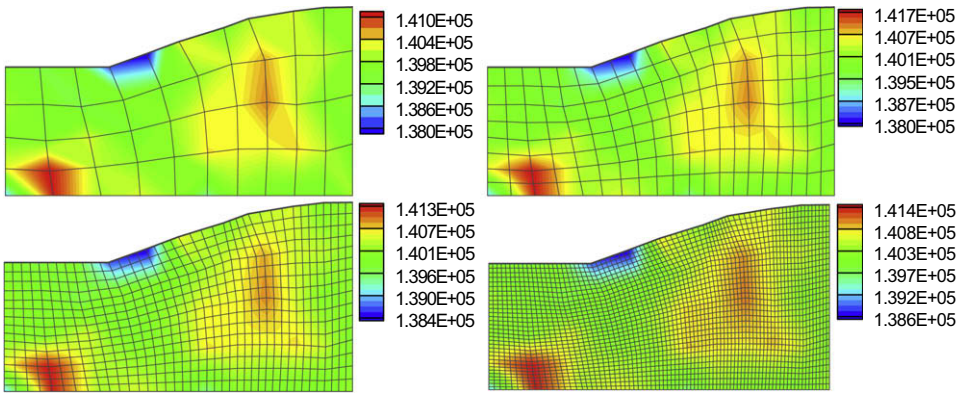

Fig. 3. Convergence of the bulk modulus (MPa) with respect to the mesh refinement in the macroscale.

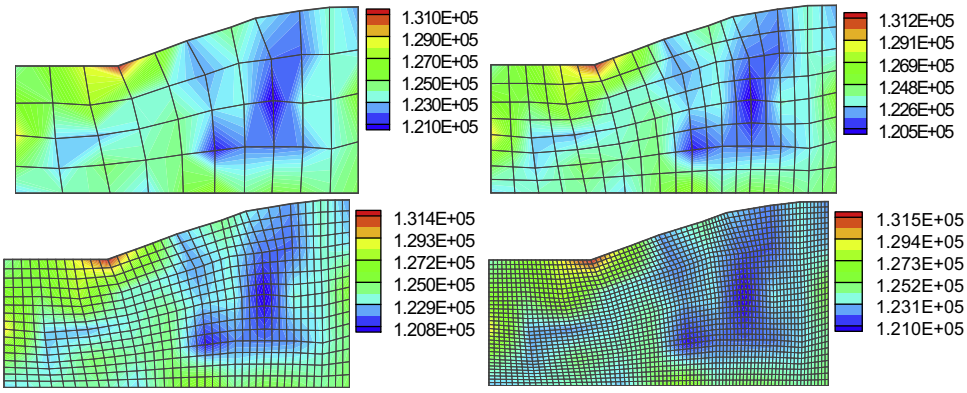

Fig. 4. Convergence of the Young's modulus (MPa) with respect to the mesh refinement in the macroscale.

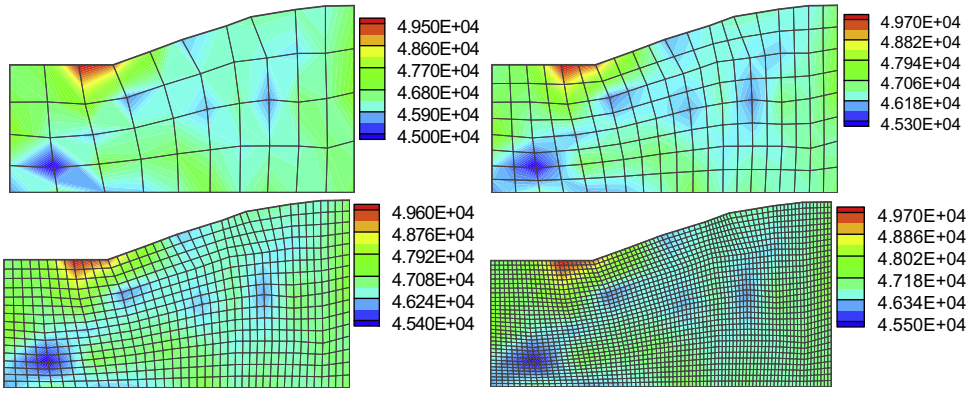

Fig. 5. Convergence of the shear modulus (MPa) with respect to the mesh refinement in the macroscale.

where the test displacement $\tilde{\boldsymbol{\eta}}$ is expressed over the initial configuration $\boldsymbol{B}_n$.

The linearization process of the homogenized PK-I stress is given as:

$$d\langle \boldsymbol{P}_r \rangle = \det \boldsymbol{F}_r \Big(\mathrm{tr}(d\boldsymbol{F}_r \boldsymbol{F}_r^{-1}) \langle \boldsymbol{T} \rangle - \langle \boldsymbol{T} \rangle (d\boldsymbol{F}_r \boldsymbol{F}_r^{-1})^T + \langle d\boldsymbol{T} \rangle \Big) \boldsymbol{F}_r^{-T} \tag{12}$$

where $d\boldsymbol{T} = d\left(\frac{1}{\det \boldsymbol{F}_r} \boldsymbol{F}_r \overline{\boldsymbol{T}} (\boldsymbol{F}_r)^T \right)$ requires the evaluation of $d\boldsymbol{F}_r$ and $d\overline{\boldsymbol{T}}$ using the constitutive model [1].

The contact problem is solved using an augmented Lagrangian framework. It is assumed that the contact problem is independent of the nature of the underlying microstructure, and that texture plays a role only through the stress response.

Note that as mentioned before each point on the macroscale corresponds to an underlying microstructure represented by another grid in Rodrigues space. Hence the material state (including texture) is updated in the sub-grid related to the microscale at each point on the macroscale. Figs. 3–5 show the convergence study of bulk, Young's and shear moduli as macroscale properties with respect to the mesh refinement on the macroscale. The material used is FCC copper as in Fig. 2 with the following elastic properties $c_{11} = 170.0$ GPa, $c_{12} = 124.0$ GPa, $c_{44} = 75.0$ GPa. For all cases, the underlying texture has been modeled by discretizing the Rodrigues

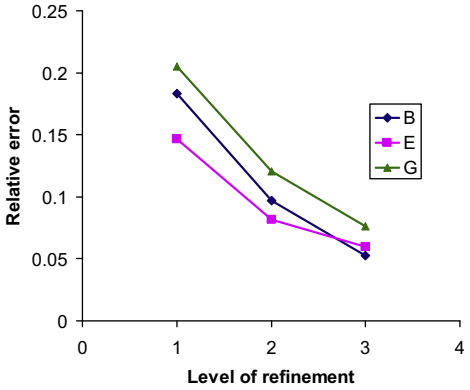

Fig. 6. Convergence of macroscale properties with respect to the level of mesh refinement.

space using 448 elements. The relative error for these macroscale properties can be written as

$$\check{E}_l := \left\| \frac{X_l - X_0}{X_0} \right\|_{L_2(D)} \tag{13}$$

where D is the spatial domain, $\check{E}_l$ is the relative error of level l ($l = 1:3$) mesh refinement with respect to level 4 mesh refinement (bottom right picture in Figs. 3–5, X_l is the value of the macroscale property for level l refinement and X_0 is the corresponding value at level 4. Fig. 6 shows this relative error with respect to the level of mesh refinement. Next, selecting level 2 mesh refinement in the macroscale, the convergence of the texture evolution for four points on the macroscale is shown in Fig. 7. Please note that the multiscale framework presented here will be used in the second example in Section 7.

3. Stochastic multiscale problem definition

The main focus of this paper is to provide a framework for quantifying the effect of random initial geometry and texture on the macroscale properties of the product in a multiscale deformation process. For this purpose, polycrystalline materials are considered.

Consider a complete probability space (Ω, F, P), where Ω is the event space, F the σ-algebra, and $P : F \to [0,1]$ is the probability measure. The uncertainty in the problem we consider comes from:

(a) The variation in the surface of the initial workpiece represented by a degree 6 Bézier curve $R_\beta(\alpha, \omega),\ \omega \in \Omega$ as

$$R_\beta(\alpha, \omega) = 0.01 \times \left(5 + \sum_{i=1}^{6} \beta_i(\omega)\varphi_i(\alpha)\right) \tag{14}$$

where $\alpha = \frac{z}{H}$ represents the z-coordinate normalized with respect to the hight of the workpiece, β_i are the Bézier coefficients and φ_i are the basis functions defined as

$$\begin{aligned}
\varphi_1(\alpha) &= (1.0-\alpha)^6 + 6\alpha(1-\alpha)^5 \\
\varphi_2(\alpha) &= 15.0(1.0-\alpha)^4\alpha^2 \\
\varphi_3(\alpha) &= 20.0(1.0-\alpha)^3\alpha^3 \\
\varphi_4(\alpha) &= 15.0(1.0-\alpha)^2\alpha^4 \\
\varphi_5(\alpha) &= 6.0(1.0-\alpha)\alpha^5 \\
\varphi_6(\alpha) &= \alpha^6
\end{aligned} \tag{15}$$

(b) Variation in the initial texture $\widehat{A}_0(x, s, \omega);\ x \in D,\ s \in \mathscr{R},\ \omega \in \Omega$, s where D is the spatial domain and $\mathscr{R}$ is the fundamental zone of the Rodrigues space. The random field $\widehat{A}_0(x, s, \omega)$ represent the variability of the initial texture.

The kinematic problem in the macroscale can be represented in the stochastic framework as

$$\widetilde{G}(\boldsymbol{u}^k_{n+1}, \tilde{\boldsymbol{\eta}}, \omega) = 0 \tag{16}$$

and the evolution of the underlying texture can be written as

$$\frac{\partial \widehat{A}(x, s, t, \omega)}{\partial t} + \widehat{A}(x, s, t, \omega) \bigtriangledown \cdot \boldsymbol{v}(s, t, \omega) = 0 \tag{17}$$

As mentioned before, finite element discretization is used for modeling the deformation process on the macroscale. Each integration point on the macroscale corresponds to an underlying texture represented in the fundamental part of Rodrigues space by a finite element discretization. So, the texture is a field at each point in the macroscale. Using a data-driven approach, the Karhunen–Loève expansion defined in subsequent sections (Eq. (22)) can be used to reduce the random field $\widehat{A}_0(x, s, \omega)$ representing the initial texture to few modes in the spatial domain and Rodrigues space. Using the finite dimensional noise assumption, the random field $\widehat{A}_0(x, s, \omega)$ can be represented by a finite number of random variables $\widehat{A}_0(x, s, \check{\xi}_1, \check{\xi}_2, \ldots, \check{\xi}_{n_d})$. In this data-driven approach, we assume that realizations of the random field $\widehat{A}_0(x, s, \omega)$ are known (from experiments or simulation) from which a reduced-order model converging in the second-order moment sense [9] to the full-order texture can be constructed. It should be noticed that the aforementioned reduced-order model is used to reconstruct the random field representing the initial texture. The reconstructed initial texture is then used to solve for the multiscale problem and the associated subproblem of texture evolution. We assume no further model reduction in the latter stage. The reduced-order model depends on n_d random variables $\check{\xi}_1, \check{\xi}_2, \ldots, \check{\xi}_{n_d}$. Rosenblatt transformation [20] can be used to transform these set of n_d random variables $\check{\xi}_1, \check{\xi}_2, \ldots, \check{\xi}_{n_d}$ to another set of n_d independent identically distributed uniform random variables $\xi_1, \xi_2, \ldots, \xi_{n_d}$ in a unit hypercube $[0,1]^{n_d}$. This allows us to sample in this space and seamlessly

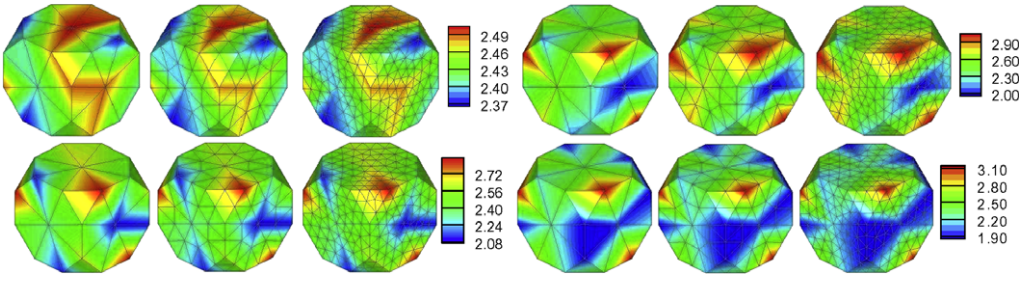

Fig. 7. Convergence of the texture evolution with respect to the number of finite elements used in the mesoscale.

use existent collocation algorithms [7] to obtain the probabilistic distribution of the final texture which in turn is used to obtain the distribution of macroscale properties.

3.1. Transforming the random variables

As discussed previously, a collocation method is used for solving the stochastic partial differential equation representing the multiscale deformation problem (see also Section 4). In this method, a unit hypercube $[0,1]^{n_d}$ represents the stochastic space where n_d is the dimension of the stochastic domain. This space is sampled using an adaptive sparse grid to compute the stochastic interpolant of the ODF. Each point in this sparse grid corresponds to a specific realization of the random variables used in constructing the reduced-order representation (described in the following sections) of the initial texture. A transformation is needed to obtain the actual random variables from the coordinates of the sparse grid points from the hypercube. This subsection provides one such transformation.

Since the joint probability density of $\breve{\xi}$ is absolutely continuous on the domain of definition, the Rosenblatt [20] transformation can be used to relate the n_d variate distribution function $P_{\breve{\xi}}$ to that of $\xi_1,\ldots,\xi_{n_d}$ which are independent identically distributed (iid) uniform random variables on the hypercube $[0,1]^{n_d}$.

$$\begin{aligned}
&\breve{\zeta}_1 = P_1^{-1}(P_{\breve{\xi}_1}(\xi_1)),\\
&\breve{\zeta}_2 = P_{2|1}^{-1}(P_{\breve{\xi}_2}(\xi_2)),\\
&\vdots\\
&\breve{\zeta}_{n_d} = P_{n_d|1:(n_d-1)}^{-1}(P_{\breve{\xi}_{n_d}}(\xi_{n_d}))
\end{aligned} \tag{18}$$

where $P_{i|1:(i-1)}$, $i=1,\ldots,n_d$, is the distribution function of $\breve{\zeta}_i$ conditioned on $\breve{\zeta}_1=\breve{\zeta}_1,\ \breve{\zeta}_2=\breve{\zeta}_2,\ \ldots,\ \breve{\zeta}_{i-1}=\breve{\zeta}_{i-1}$ obtained from $P_{\breve{\zeta}}$. This would help in seamlessly incorporating the collocation strategy described in the next section to solve the stochastic partial differential equation under study.

4. Sparse grid interpolation: uncertainty propagation

For obtaining the macroscale properties one needs the underlying texture. This section provides a summary of the algorithm used in obtaining the effect of uncertainty on texture evolution. An adaptive sparse grid collocation strategy for constructing the stochastic solution for the evolution of the ODF is used. For details, the interested reader is referred to [7].

The basic idea of the stochastic collocation method is to approximate the stochastic space using multi-dimensional interpolating functions. The method uses realizations of the function (i.e. the solution $\widehat{A_f}(x,s,\xi_i)$ of the SPDE Eq. (17), at a finite set of collocation points $\{\xi_i\}_{i=1}^{n_n}$, where the evolved texture is shown by $\widehat{A_f}$ and n_n is the number of collocation points). These finite number of deterministic solutions are used in constructing an interpolant of the ODF using hierarchical linear interpolating basis functions [7]. The sparse grid is based on the Newton–Cotes formulae using equidistant support nodes [7]. The sampling points on the hypercube ($\Gamma=[0,1]^{n_d}$, where n_d is the number of stochastic dimensions) are defined using tensor products and following the Smolyak construction. The function $\widehat{A_f}(x,s,\xi)$ is approximated as follows:

$$\widehat{A_f}(x,s,\xi_i) = \sum_{|i|\leqslant q}\sum_j \theta_j^i(x,s)\cdot a_j^i(\xi) \tag{19}$$

where for each point on the macroscale there is a sparse grid interpolant which represents the random texture at each discretized point in Rodrigues space. This is just a simple weighted sum of the value of the basis functions for all collocation points in the current sparse grid where $a_j^i \equiv a_j(\xi_j^i)$ are the n_d-dimensional multilinear basis functions, θ_j^i are the so called hierarchical surpluses (difference between the value of interpolant in the current and previous interpolation level), $q-n_d$ is the order of interpolation, n_d is the number of stochastic dimensions and the summation is over the collocation points [7].

After obtaining the expression in Eq. (19), it is easy to extract statistics [7]. For example, the mean of the random solution can be evaluated as follows:

$$E[\widehat{A_f}(x,s,\xi)] = \sum_{|i|\leqslant q}\sum_j \theta_j^i(x,s).\int_\Gamma a_j^i(\xi)d\xi \tag{20}$$

where the probability density function $p(\xi)$ is 1 since the stochastic space is a unit hypercube $[0,1]^{n_d}$. As shown in [7], the multi-dimensional integral is simply the product of the corresponding 1D integrals which can be computed analytically. The second-order moment can be calculated by also constructing a sparse grid interpolant for $\widehat{A_f}^2(x,s,\xi)$. Higher-order statistics including the PDF can be calculated by sampling from the interpolant.

5. A multiscale reduced-order model of the uncertain initial microstructure

This section provides a framework to obtain a reduced-order model for the underlying random microstructure field (here ODFs defining texture). Assume an L^2 random field $\breve{a}(x,s,\omega)$ defined on a probability space (Ω,F,p)

$$\breve{a}(x,s,\omega): D\times\mathscr{R}\times\Omega\to\mathbb{R} \tag{21}$$

where D is the spatial domain, $\mathscr{R}$ is the fundamental part of Rodrigues space, Ω is the set of elementary events and $\omega\in\Omega$ is the vector of random inputs. One can use the Karhunen–Loève expansion to express this field by a bi-orthogonal representation in the form

$$\begin{aligned}
\breve{a}(x,s,\omega) &= \bar{a}(x,s)+\hat{a}(x,s,\omega)\\
&= \bar{a}(x,s)+\sum_{i=1}^{\infty}\sqrt{\rho_i}\psi_i(s)\Phi_i(x,\omega)
\end{aligned} \tag{22}$$

where $\bar{a}$ is defined as $\bar{a}(x,s)=\langle\breve{a}(x,s,\omega)\rangle$ and $\langle\cdot\rangle$ is the averaging operation defined below, ρ_i are eigenvalues of the eigenvalue problem defined later on, the ψ_i are modes strongly orthogonal in Rodrigues space, Φ_i are spatial modes weakly orthogonal in space with respect to an inner product defined as

$$(f,g) := \int_D \langle f,g\rangle dx \tag{23}$$

$$\langle f,g\rangle = \int f(\omega)g(\omega)p(\omega)d\omega \tag{24}$$

where $p(\omega)$ is the probability distribution. The strong orthogonality of ψ_i modes in Rodrigues space can be written as

$$(\psi_i,\psi_j)_{\mathscr{R}} = \int_{\mathscr{R}}\psi_i(s)\psi_j(s)ds = \delta_{ij} \tag{25}$$

and the weak orthogonality of spatial modes can be written as

$$(\Phi_i,\Phi_j) = \delta_{ij} \tag{26}$$

By minimizing the distance (based on the norm defined in Eq. (23)) between the Karhunen–Loève expansion and the random field, one ends up with [9]

$$\psi_i(s) = \frac{1}{\sqrt{\rho_i}}(\hat{a},\Phi_i) \tag{27}$$

and from the orthogonality condition

$$\Phi_i(x,\omega) = \frac{1}{\sqrt{\rho_i}}\int_{\mathscr{R}}\hat{a}(x,s,\omega)\psi_i(s)ds \tag{28}$$

Eqs. (27) and (28) lead to the following eigenvalue problem:

$$\rho_i \psi_i(s) = \int_{\mathscr{R}} C(s,\acute{s})\psi_i(\acute{s})d\acute{s} \tag{29}$$

where the covariance C is defined as

$$C(s,\acute{s}) = (\hat{a}(x,s,\omega),\hat{a}(x,\acute{s},\omega)) \tag{30}$$

In discrete form, the covariance can be written as

$$\boldsymbol{C} = \frac{1}{n_r}\sum_{j=1}^{n_r}\sum_{i_n=1}^{n_{el}}\sum_{i_m=1}^{n_{int}} \hat{\boldsymbol{a}}_j(x_{i_m})\hat{\boldsymbol{a}}_j^T(x_{i_m})\hat{\eta}_{i_m}|J_{i_n}| \tag{31}$$

where $|J_{i_n}|$ is the Jacobian determinant of the element i_n, $\hat{\eta}_{i_m}$ is the integration weight associated with the integration point i_m, n_{int} is the number of integration points in each element, n_r is the number of realizations, n_{el} is the number of elements in macroscale and $\hat{\boldsymbol{a}}$ is a column vector with elements corresponding to integration points in Rodrigues space and x_{i_m} represents global coordinate of the integration point i_m in macroscale.

It should be noticed that the choice of inner product defined in Eq. (23) is not unique. In [9], three different inner products were explored out of which the one minimizing the second-order moment of the error (the distance between the Karhunen–Loève expansion and the random field) is adopted in here. Also note that in Eq. (25), $ds = ds_1 ds_2 ds_3$ but the integration in still in Rodrigues space. One can equivalently use $d\nu = (\det g)^{0.5} ds_1 ds_2 ds_3$ in the integration in Eq. (25) with appropriate scaling of the covariance matrix C and the eigenvectors ψ_i.

The ODF representing the texture takes positive values. Hence, the Karhunen–Loève expansion should provide us with positive values. To obtain a positive random field, one can use the Karhunen–Loève expansion for the $\breve{a}(x,s,\omega) = log(\widehat{A}(x,s,\omega) - A_{min})$ assuming that $\widehat{A}(x,s,\omega) > A_{min} > 0$ almost surely [21]. The process $\widehat{A}$ can be reconstructed as

$$A_{min} + exp(\breve{a}(x,s,\omega)) = A_{min} + exp(\bar{a}(x,s) + \sum_i \times \sqrt{\rho_i}\psi_i(s)\Phi_i(x,\omega)) \tag{32}$$

It should be noticed that as shown in Eq. (4), the significance of the values for each component of the texture $\widehat{A}$ can be determined relative to its other components. In cases that the texture is constructed such that it approximates the distribution of orientations from a realistic picture of microstructure (schematically shown in Fig. 1) some elements of $\widehat{A}$ can be zero due to absence of the specific orientation in the picture. In this case, a small number compared to other components of $\widehat{A}$ should be provided instead of zero to avoid obtaining an unbounded $\hat{\boldsymbol{a}}$. Although a more robust method to tackle this problem is presented in [12], more mathematical developments are still needed to apply it to the multiscale case.

In practice, $\breve{a}(x,s,\omega) := \breve{a}(x,s,\xi_1(\omega),\ldots,\xi_{n_d}(\omega))$, where $\xi_1,\ldots,\xi_{n_d}$ are a set of finite number of random variables and n_d refers to the number of random variables considered in the problem.

Next, the polynomial chaos decomposition of $\Phi_i(x,\omega)$ can be written as

$$\Phi_i(x,\omega) := \Phi_i(x,\zeta_1(\omega),\ldots,\zeta_{n_d}(\omega)) = \sum_j \phi_{ij}(x)\eta_j(\omega) \tag{33}$$

where the $\eta_i(\omega) = \eta_i(\zeta(\omega))$ are in a one-to-one correspondence with the Hermite polynomials in Gaussian variables (see Section 6), $\zeta(\omega)$ is the vector consisting of n_d independent Gaussian random variables $(\zeta_1,\ldots,\zeta_{n_d})$ and the coefficients $\phi_{ij}(x)$ can be obtained from

$$\phi_{ij}(x) = \frac{\langle \Phi_i(x,\zeta)\eta_j\rangle}{\langle \eta_j^2\rangle} \tag{34}$$

It should be noticed that in order to calculate the right hand side of the above equation, Φ_i and η should be expressed in the same probability space. But Φ_i obtained from Eq. (28) is expressed with respect to ξ (Eq. (19)) i.e. each realization of Φ_i is with respect to a set of n_d independent uniformly distributed random variables (recall that Φ_i was constructed from realizations of texture by sampling on the hyprecube). A simple transformation as Eq. (18) can transform these random variables to a set of n_d independent Gaussian random variables $(\zeta_1,\ldots,\zeta_{n_d})$ with mean zero and variance one.

6. Polynomial chaos expansion

A second-order process can be approximated by a series of terms of Hermite polynomials in Gaussian variables. This approximation is mean-square convergent. If $\Phi_i(x,\omega)$ is a second-order random process $\langle \Phi_i(x,\omega),\Phi_i(x,\omega)\rangle < \infty$, it can be written as an expansion in terms of Hermite polynomials $H_n(\zeta_{i_1},\ldots,\zeta_{i_{n_d}})$ of order n in the Gaussian variables $(\zeta_{i_1},\ldots,\zeta_{i_{n_d}})$ with zero mean and unit variance, where i indexes the modes in Eq. (22) and $i_1, i_2, \ldots$ index the polynomial terms. This expansion is usually written as

$$\Phi_i(x,\omega) = \sum_{j=0}^{\infty} Y_{ij}(x)\eta_j(\zeta) \tag{35}$$

where there is a one-to-one correspondence between $H_n(\zeta_{i_1},\ldots\zeta_{i_{n_d}})$ and $\eta_j(\zeta_{i_1},\ldots\zeta_{i_{n_d}})$. In practice this series can be truncated with respect to the order of Hermite polynomials and the dimension of the random vector ζ. The Hermite polynomials are orthogonal with respect to the Gaussian probability measure.

If the dimension of the random vector ζ is n_d and the order of Hermite polynomials is p the total number of terms in polynomial chaos expansion is $P+1$.

$$P+1 = \frac{(p+n_d)!}{p!n_d!} \tag{36}$$

The dimension of the random vector ζ in polynomial chaos is dictated by the number of random variables driving the stochastic problem and the order of Hermite polynomials is decided from a convergence study on the probability distribution of the random process $\Phi_i(x,\omega)$.

6.1. Computational aspects of polynomial chaos expansion

In order to obtain the coefficients of the polynomial chaos using Eq. (34), one can use the sampling method in which the sample values of $\zeta = (\zeta_1,\zeta_2,\ldots,\zeta_{n_d})$ are drawn from the distribution of the ζ which in this case is the n_d-dimensional independent Gaussian distribution.

For each sampling point, $\eta_i(\zeta)$ and $\Phi_i(x,\zeta)$ are evaluated. Using all the samples, one can evaluate the expectation in the nominator of the Eq. (34). If the dimension of the stochastic space is large, the best strategy for sampling are Monte-Carlo or Latin hypercube methods. The expectation in the denominator of Eq. (34) can be calculated and tabulated offline. For examples on the first few of the latter expectations, one can refer to [5]. A more elegant and efficient way of calculating the expectations of the form $\langle \Phi(x,\zeta)\eta(\zeta)\rangle$ is to resort to Gauss–Hermite quadrature methods. This method is efficient for small dimensions of the stochastic space. In this method, the expectation operator $\langle f\rangle$ is approximated as $\sum_i w_i f_i$, where w_i are the weights in the Gauss–Hermite quadrature method. If polynomial chaos expansion of order p is sufficient to represent the random process under study, then $p+1$ sample points on each stochastic domain are needed for calculation of the $\langle f\rangle$. The sample points for the multi-dimensional stochastic space are constructed from the sample points on each stochastic

dimension using tensor product. The sample points on each stochastic dimension are the roots of the Hermite polynomial H_{p+1}.

For the one-dimensional case, one can write

$$\langle f\rangle = \int_{-\infty}^{+\infty} \frac{1}{\sqrt{2\pi}} e^{-\frac{\zeta^2}{2}} f(\zeta)d\zeta = \frac{1}{\sqrt{2\pi}} \int_{-\infty}^{+\infty} e^{-\zeta^2} e^{\frac{\zeta^2}{2}} f(\zeta)d\zeta \sim \sum_{i=1}^{p+1} w_i f(\acute{x}_i) \tag{37}$$

where $\acute{x}_i$ are roots of the Hermite polynomial H_{p+1} and the associated weights are given by

$$w_i = \frac{2^p (p+1)!\sqrt{\pi}}{(p+1)^2 [H_p(\acute{x}_i)]^2} \times \frac{1}{\sqrt{2\pi}} e^{\frac{\acute{x}_i^2}{2}} \tag{38}$$

For the multi-dimensional stochastic space with dimension n_d these weights can be calculated using the multiplication of $w_1, \ldots, w_{n_d}$ calculated for each dimension at the corresponding coordinate of the sampling point.

6.2. Summary of the algorithm

First, let us look at the method used in [13]. Assume the information on the texture is given through realizations of the texture for each integration point on the macroscale. There for each integration point, one can write the following:

$$\breve{a}_1(s,\omega) = \bar{a}_1(s) + \sum_{i_1=1}^{\infty} \sqrt{\rho_{i_1}} \psi_{i_1}(s) \breve{\alpha}_{i_1}(\omega) \tag{39}$$

$$\breve{a}_2(s,\omega) = \bar{a}_2(s) + \sum_{i_2=1}^{\infty} \sqrt{\rho_{i_2}} \psi_{i_2}(s) \breve{\alpha}_{i_2}(\omega)$$

$$\vdots$$

$$\breve{a}_j(s,\omega) = \bar{a}_j(s) + \sum_{i_j=1}^{\infty} \sqrt{\rho_{i_j}} \psi_{i_j}(s) \breve{\alpha}_{i_j}(\omega)$$

$$\vdots$$

where $\breve{a}_j(s,\omega)$ is the value of the random field corresponding to the integration point j, $\bar{a}_j$ is the expectation of the random field at integration point j, ρ_{i_j} and $\psi_{i_j}(s)$ are the eigenvalues and eigenfunctions in Rodrigues space and $\breve{\alpha}_{i_j}(\omega)$ are the set of uncorrelated but not necessarily independent random variables at integration point j. In this framework, the realizations of the random variables at each integration point are obtained using

$$\breve{\alpha}_{i_j}(\omega) = \frac{1}{\sqrt{\rho_{i_j}}} \int_{\mathscr{R}} \breve{a}_j(s,\omega) \psi_{i_j}(s) ds \tag{40}$$

Using these realizations, one can use methods like the one presented in [12] to construct the probability distributions of these random variables at each integration point j. Now if the random variables at different integration points are correlated to each other then the aforementioned methodology has no means of figuring that out, in another words it cannot see the correlation between the set of random variables from different integration points. So, the number of random variables one would end up with would be the number of random variables needed for each integration point multiplied by the number of integration points. But if in a problem we know that the number of random variables driving the problem is much less than the aforementioned value then one should think of alternative methods. To address this problem one can use the method presented in this paper. A summary of the proposed algorithm is given in here:

The random field can be approximated as:

$$\hat{a}(x,s,\omega) = \sum_{i=1}^{\infty} \sqrt{\rho_i} \psi_i(s) \Phi_i(x,\omega) \tag{41}$$

where ρ_i, $\psi_i(s)$ are the eigenvalues and eigenfunctions (modes in Rodrigues space) of the covariance C. After constructing the covariance matrix and obtaining its eigenvalues and eigenfunctions the random spatial modes $\Phi_i(x,\omega)$ corresponding to each mode in Rodrigues space can be obtained by the following projection:

$$\Phi_i(x,\omega) = \frac{1}{\sqrt{\rho_i}} \int_{\mathscr{R}} \hat{a}(x,s,\omega) \psi_i(s) ds \tag{42}$$

Once the random spatial modes have been obtained, they are decomposed to spatial and random space using polynomial chaos decomposition

$$\Phi_i(x,\omega) = \sum_j \phi_{ij}(x) \eta_j(\omega) \tag{43}$$

where $\eta_j(\omega)$ are Hermite polynomials in Gaussian variables with the dimension equal to the number of random variables driving the stochastic problem and the order obtained from a study on convergence of the decomposition and $\phi_{ij}(x)$ are coefficients of the decomposition which vary from one integration point to another and can be calculated using

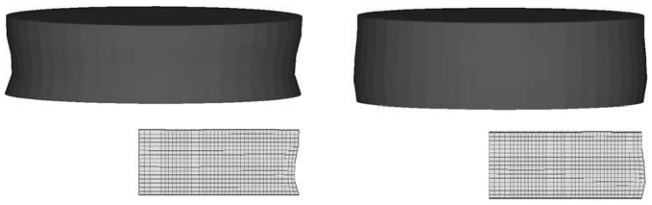

Fig. 8. Two samples of the perturbed initial geometry.

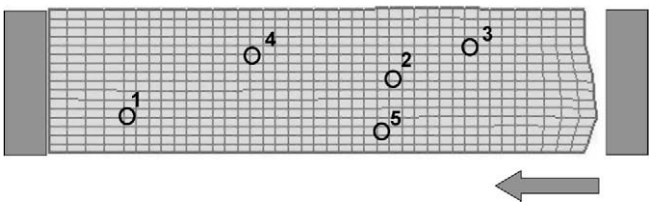

Fig. 9. A sample of workpiece. The numbered points are investigated in subsequent figures.

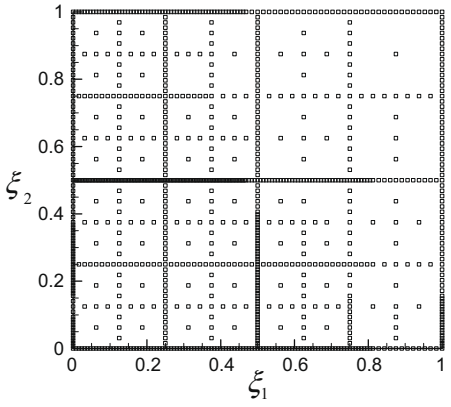

Fig. 10. Sparse grid collocation points spanning the stochastic space of random Bézier parameters.

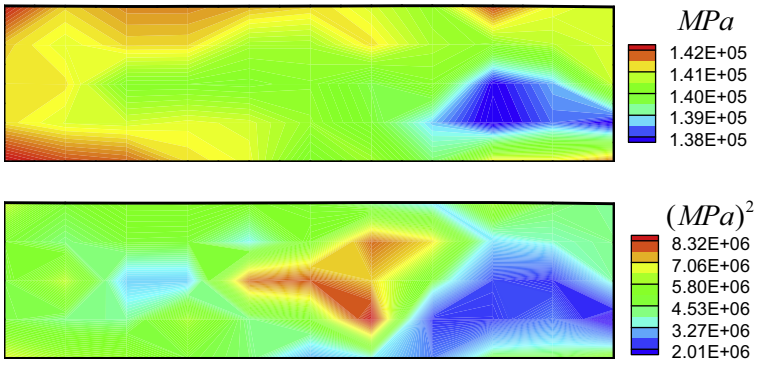

Fig. 11. Mean and variance of the bulk modulus.

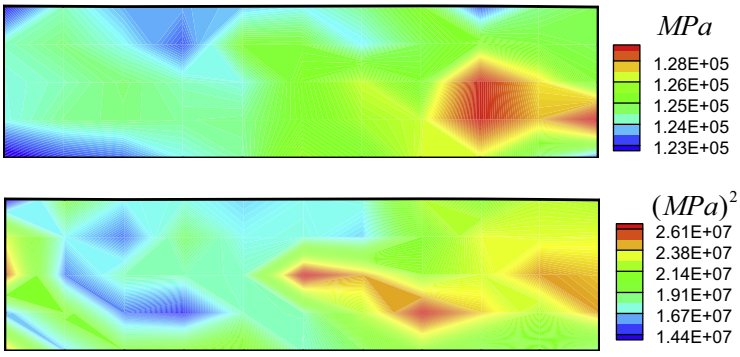

Fig. 12. Mean and variance of the Young's modulus.

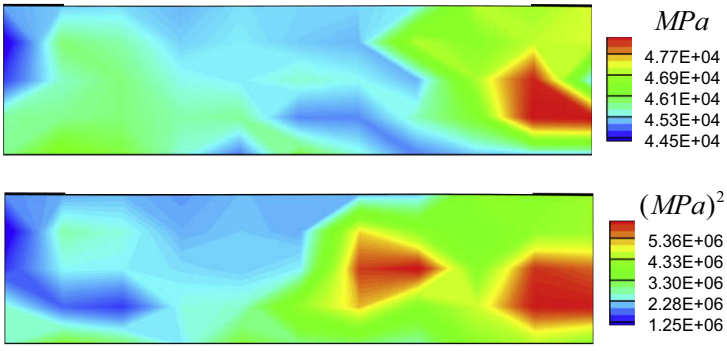

Fig. 13. Mean and variance of the shear modulus.

$$\phi_{ij}(x) = \frac{\langle \Phi_i(x,\zeta)\eta_j \rangle}{\left\langle \eta_j^2 \right\rangle} \tag{44}$$

Now that all the components of Eq. (41) are known, it can be used to reconstruct the random field. Notice that the realizations of the random field were used to construct the covariance matrix. Hence, Eq. (41) represents the underlying random field and its realizations can be reconstructed as many times as needed using the realizations of the random variables in the Hermite polynomials.

Finally note that a convergence study has been conducted to find the order of the Hermite polynomials but this has been done assuming a fixed dimension for the random space. Selection of the optimal stochastic dimensionality in the bio-orthogonal decomposition to represent the given snapshots of texture at different points on the macroscale was not addressed here. A simple approach to this problem may involve a progressive increase in the stochastic dimensionality until the given data are represented best. Such approach was not considered here (where a priori knowledge was used to select the stochastic dimensionality) due to the high computational cost involved.

7. Numerical examples

7.1. Example 1

In this example, the effect of uncertainty in the geometry of the initial workpiece on the macroscale properties of the product of a deformation process is investigated. It is assumed that the surface of the initial workpiece $R_\beta(\alpha,\omega)$ can be represented by a degree 6 Bézier curve (Eq. (14)).

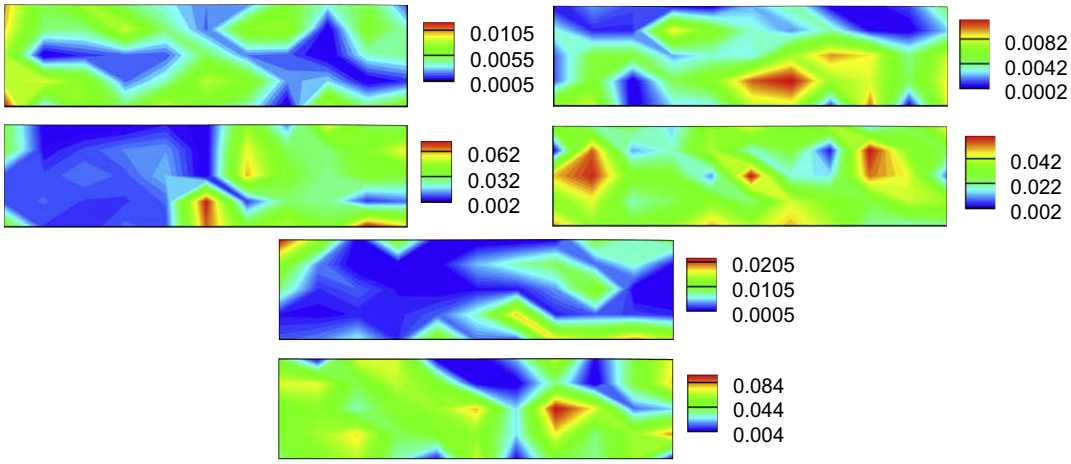

Fig. 14. Comparison of the mean and variance of the macroscale properties with MC (relative error). Top left: bulk modulus, top right: Young's modulus, bottom: shear modulus.

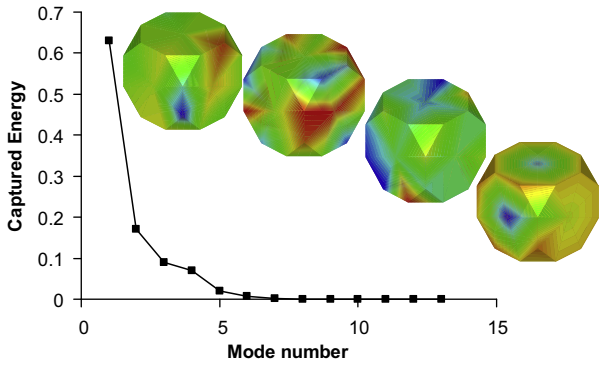

Fig. 15. Eigenvalues and eigenvectors from the bio-orthogonal decomposition of the texture data.

In this problem, the Bézier coefficients β_1, β_4, β_5, β_6 are assumed to be deterministic ($\beta_i = 0.05$; $i = \{1,4,5,6\}$) and β_2, β_3 are considered as two independent random variables following $N(1, 0.1)$ distribution. If all the Bézier coefficients are equal to 0.05 the resulting cylinder will have radius 5.5 cm. Fig. 8 shows few examples of workpieces constructed using realizations of β_2 and β_3. The workpiece is subjected to a forging process with forging velocity specified as 0.01 cm/s and when forged using a closed forming die depicted in Fig. 9 the final product will be a cylinder of radius 4.0 cm. The material considered here is FCC copper as before.

For all points on the macroscale the underlying initial texture is assumed to be constant ($A_0(x,s) = 2.435$). This correspond to a texture having the same volume fraction for all possible orientations. Although the initial texture is assumed to be deterministic in this problem, the evolved texture at the end of the deformation process

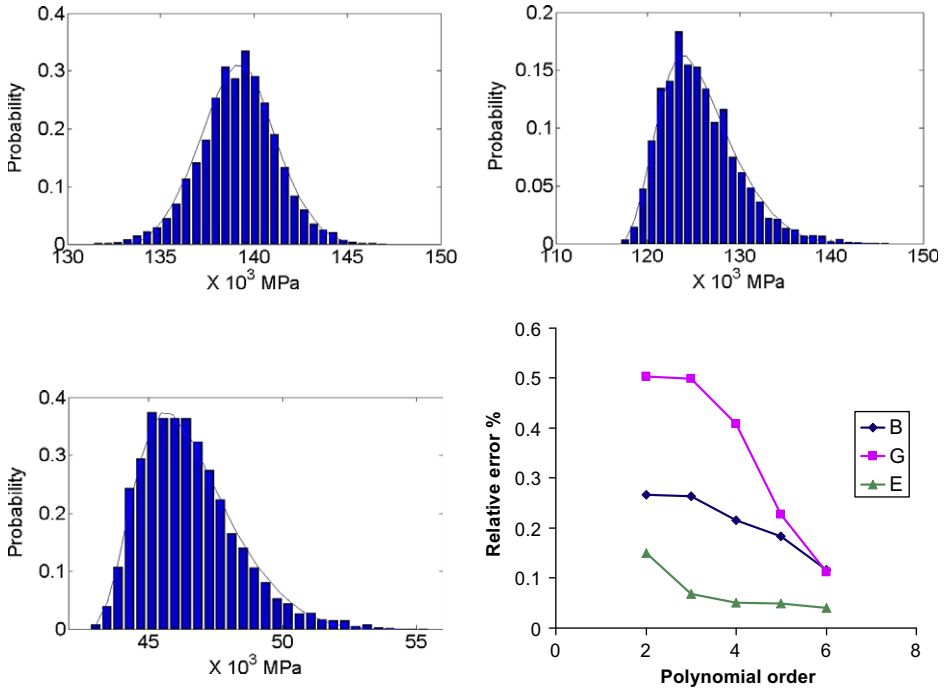

Fig. 16. Top left: distribution of bulk modulus, top right: distribution of Young's modulus, bottom left: distribution of shear modulus, bottom right: the relative error of macroscale properties with respect to the order of polynomial chaos used in the approximation (for Point 1 on macroscale).

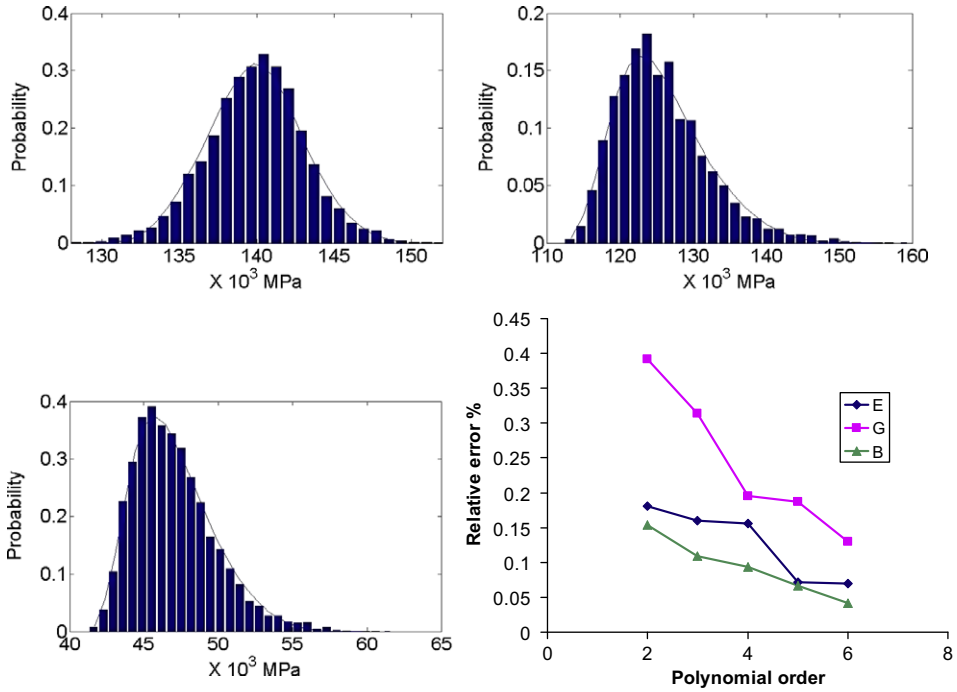

Fig. 17. Top left: distribution of bulk modulus, top right: distribution of Young's modulus, bottom left: distribution of shear modulus, bottom right: the relative error with respect to the order of polynomial chaos (for Point 2 on macroscale).

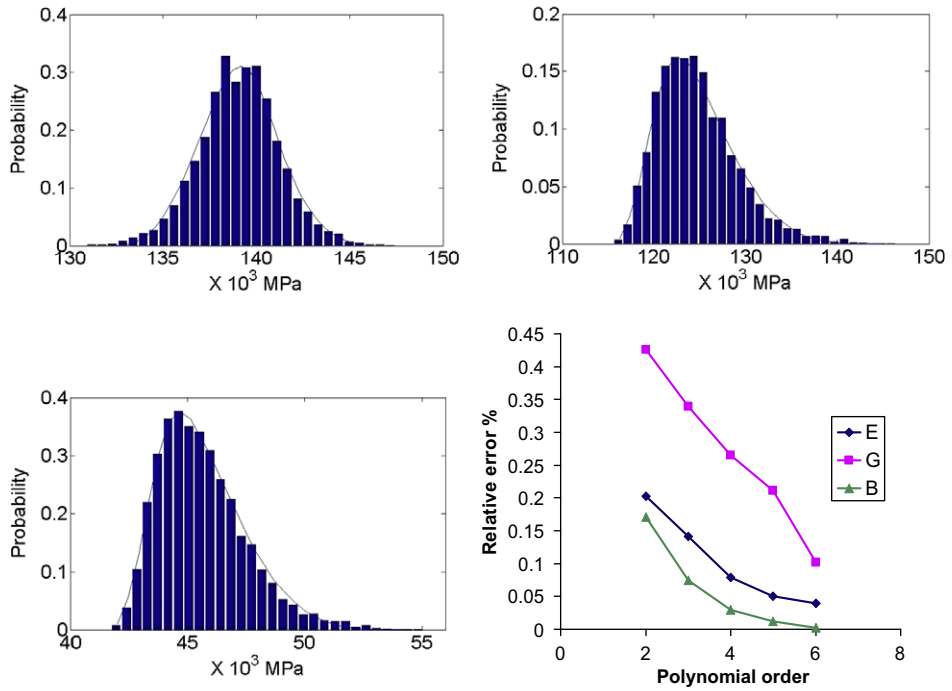

Fig. 18. Top left: distribution of bulk modulus, top right: distribution of Young's modulus, bottom left: distribution of shear modulus, bottom right: the relative error with respect to the order of polynomial chaos (for Point 3 on macroscale).

will be random due to the random initial geometry for the workpiece and the propagation of uncertainty through the deformation process.

A level 8 interpolating adaptive sparse grid corresponding to 1368 points for this particular stochastic problem has been used. The coordinates of the collocation points are shown in Fig. 10. The coordinates of each collocation point correspond to the variables ξ_1 and ξ_2 which are independent uniformly distributed random variables between 0 and 1. These two random variables are mapped to β_2 and β_3 using the Rosenblatt transformation (Eq. (18)). An approximation is made in this step in which the tails of the normal probability distribution are cut at values equal to the

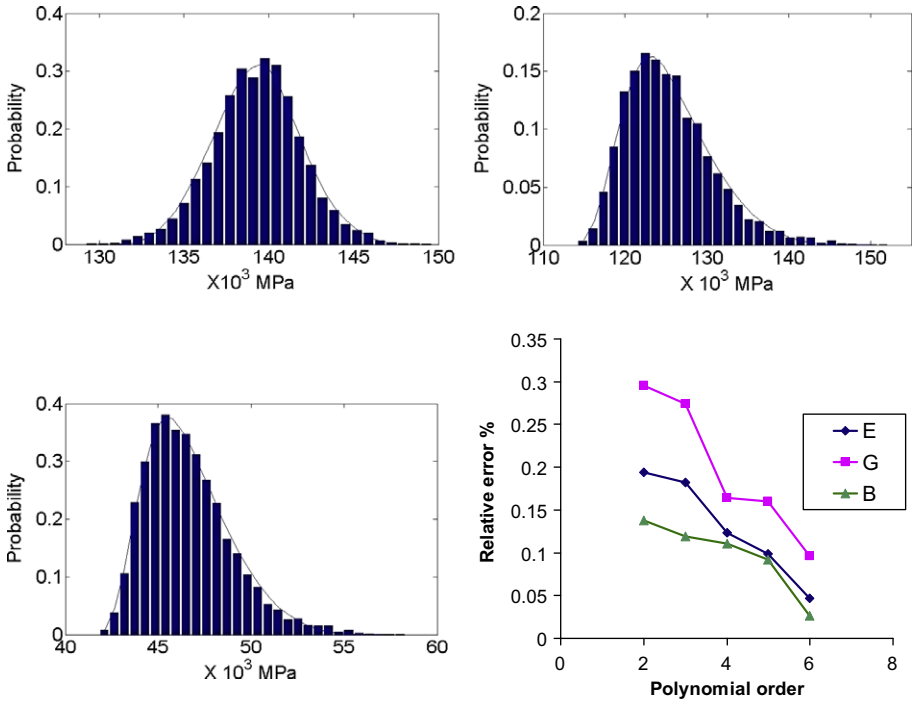

Fig. 19. Top left: distribution of bulk modulus, top right: distribution of Young's modulus, bottom left: distribution of shear modulus, bottom right: the relative error with respect to the order of polynomial chaos (for Point 4 on macroscale).

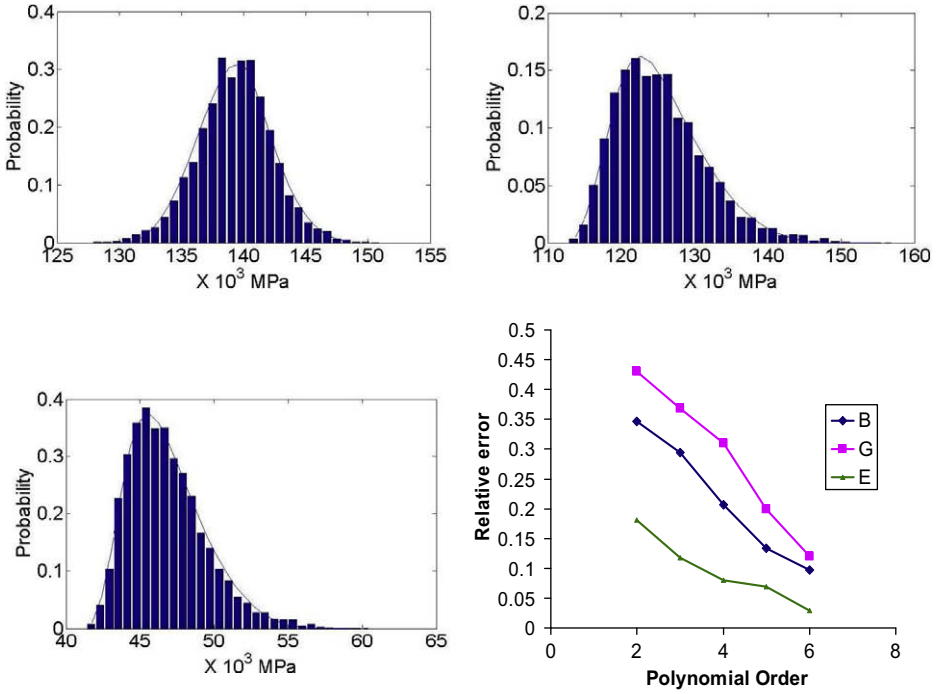

Fig. 20. Top left: distribution of bulk modulus, top right: distribution of Young's modulus, bottom left: distribution of shear modulus, bottom right: the relative error with respect to the order of polynomial chaos (for Point 5 on macroscale).

($mean \pm 6 \times std$), where *std* is the standard deviation. This approximation is to avoid the infinite values for β corresponding to $\xi_1,\ \xi_2 = 0$ or 1. Cutting the tails of the probability distribution has negligent effect on the properties under study (mean and variance of the macroscale properties). The mean and variance of the bulk, Young's and shear moduli are shown in Figs. 11–13, respectively. The same problem has been solved using Monte-Carlo (MC) method with a relatively small (4000) number of samples. As expected, the error is bigger for the variance rather than the mean but overall the results from both methods agree quite well. The relative errors between the mean and the variance obtained from these two methods are shown in Fig. 14. The relative error used in these figures can be written as $E_r = \left|\frac{X - X_{MC}}{X_{MC}}\right|$, where X is the

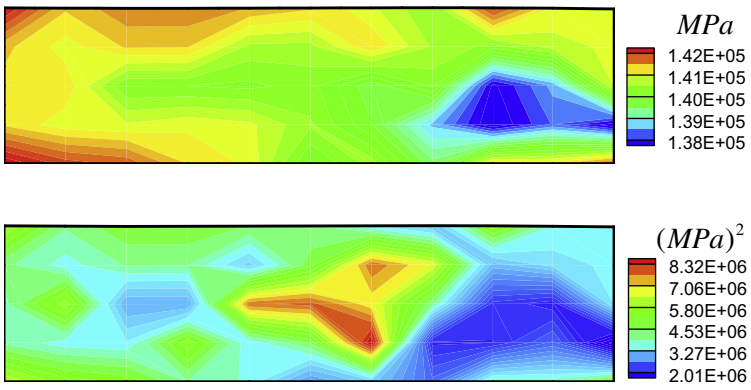

Fig. 21. Mean and variance of the bulk modulus obtained from the reduced-order representation of texture.

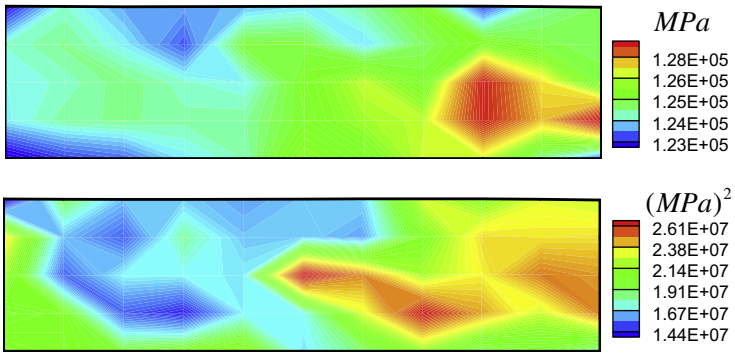

Fig. 22. Mean and variance of the Young's modulus obtained from the reduced-order representation of texture.

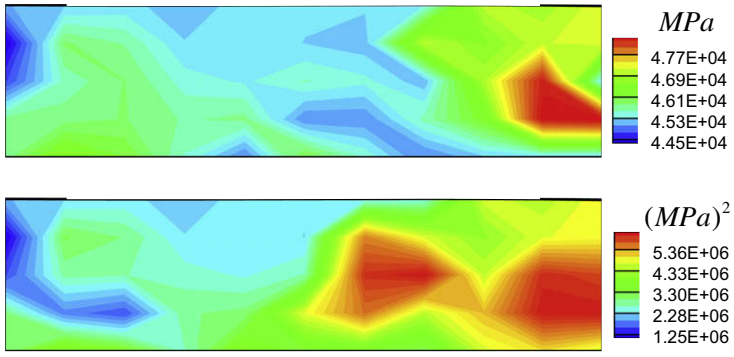

Fig. 23. Mean and variance of the shear modulus obtained from the reduced-order representation of texture.

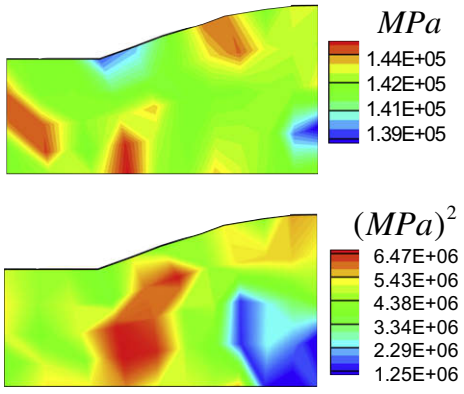

Fig. 24. Mean and variance of the bulk modulus obtained from the reduced-order representation of texture.

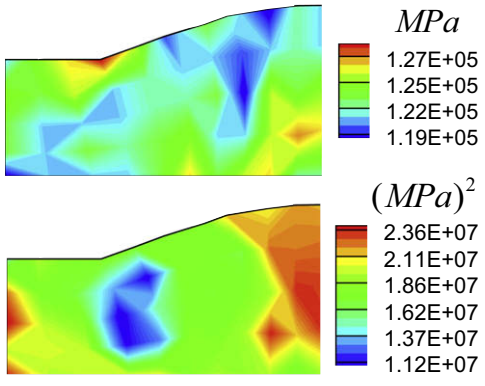

Fig. 25. Mean and variance of the Young's modulus obtained from the reduced-order representation of texture.

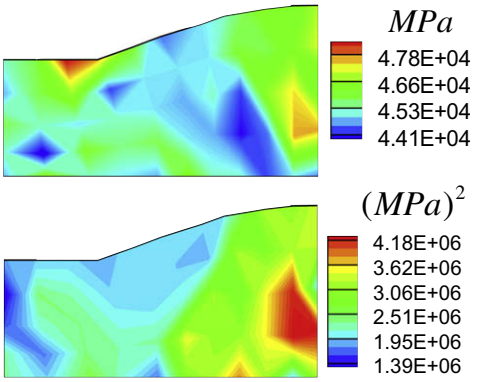

Fig. 26. Mean and variance of the shear modulus obtained from the reduced-order representation of texture.

macroscale property calculated using the samples of texture obtained from the interpolants resulting from the sparse grid collocation method and X_{MC} is the corresponding macroscale property obtained from Monte-Carlo.

Next, a reduced-order representation of texture is constructed using Eq. (22). First, the covariance matrix C is calculated using Eq. (31). The first few eigenvalues and eigenvectors of this matrix are shown in Fig. 15.

Using the first six significant modes in Fig. 15, the spatial modes $\Phi_i(x,\omega)$ are calculated using Eq. (28). Next, Eq. (34) is used to obtain the polynomial chaos approximation of $\Phi_i(x,\omega)$. Having the reduced-order representation, using Eqs. (22) and (32), 50,000 sample textures are constructed for the macroscale points. The bulk, Young's and shear moduli for these reconstructed textures are calculated and compared to the values obtained with the full-order texture in Figs. 16–20. These figures correspond to macroscale points 1–5, respectively, shown in Fig. 9. In these figures, the top left plot represents the distribution of the bulk modulus while the top right and bottom left show the distribution of Young's modulus and shear modulus, respectively. Also, the bars represent the distribution of the corresponding macroscale property calculated from samples of the texture obtained from the interpolant constructed by sparse grid collocation (Eq. (19)). The solid line shows the distribution of the same property calculated from the samples obtained from the reduced representation of the texture. The percentage of the relative error defined as $\widetilde{E} := \|(X^{p+1} - X^p)/X^{p+1}\|_{L_2(\Omega)}$ is also shown vs. polynomial order in the aforementioned figures.

Figs. 21–23 show the mean and the variance for the bulk, Young's and shear moduli, respectively, on the macroscale using samples of textures reconstructed from the reduced-order model. Reasonable match has been achieved in comparison to Figs. 11–13.

7.2. Example 2

The final texture of Example 1 is used as the initial texture in this example. It should be noticed that except using the knowledge from the first example on having a stochastic space with rank 2 there is no connection between these two examples. Example 2 deals with one stage deformation process with the random initial texture computed in Example 1. The reader is reminded that using the method in [13] for the same amount of knowledge (realizations of the texture at each integration point on the macroscale and knowledge of the rank of the stochastic space) one will end up with independent random variables for each integration point without exploiting the correlation between them.

As described in the previous example, Eq. (22) is used to construct a reduced-order representation of the random process $A_0(x,s,\omega)$. In this case, the first six eigenmodes of the covariance matrix C (Eq. (31)) were used and for each of these eigenmodes, Eq. (28) is used to construct the spatial eigenmodes. An order six polynomial chaos expansion is used to approximate these spatial

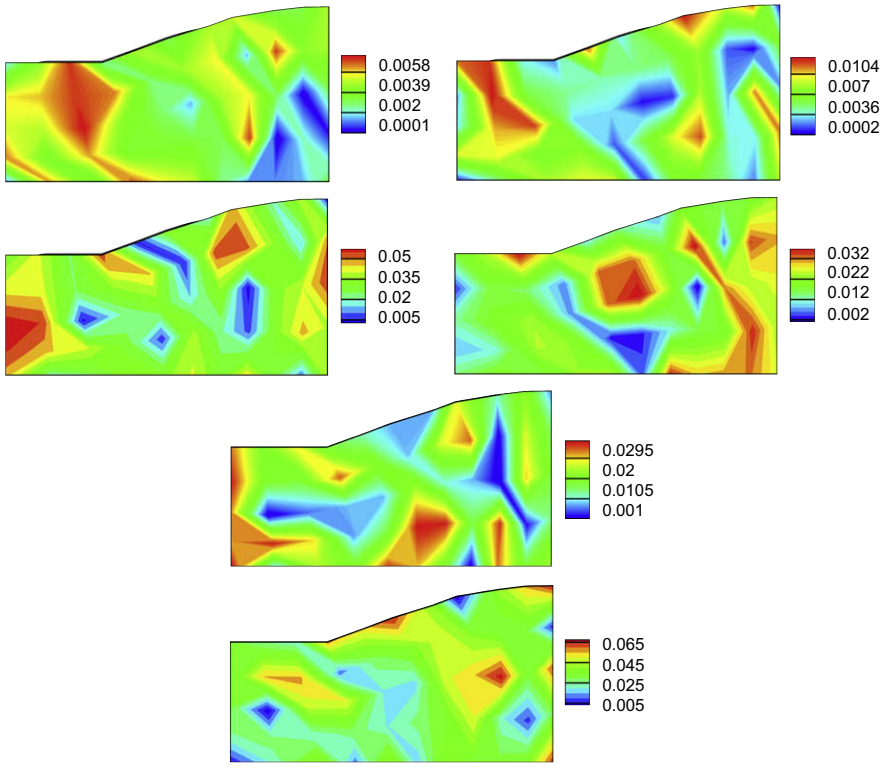

Fig. 27. Comparison of mean and variance of the macroscale properties with MC (relative error). Top left: bulk modulus, top right: Young's modulus, bottom: shear modulus.

eigenmodes and the dimension of the random vector ζ is the same as the dimension of the random vector driving the first example (i.e. $dim(\zeta) = 2$). Thus using Eq. (36), it is obvious that for each point on the macroscale and for each eigenmode in Rodrigues space, a set of 28 polynomial coefficients are used. These coefficients along with the eigenmodes and eigenvectors of covariance C (Eq. (31)) are used to reconstruct the random process $A_0(x, s, \omega)$ representing the initial texture of Example 2.

The workpiece and the die are as depicted in Fig. 1 and the forging velocity is considered to be 0.01 cm/s. When solving this problem using sparse grid collocation, the coordinates of each point on the sparse grid correspond to ξ_1 and ξ_2 which are two independent uniformly distributed random variables. Rosenblatt transform (Eq. (18)) is used to transform these to ζ_1 and ζ_2 which follow an $N(0, 1)$ distribution. ζ_1 and ζ_2 are in turn used to construct samples of $\Phi(x, \omega)$ using Eq. (33) and finally Eqs. (22) and (32) were used to construct the corresponding realization of $A_0(x, s, \omega)$ that would be used as the initial texture of the workpiece.

Figs. 24–26 show the mean and variance of the bulk, Young's and shear moduli obtained at the end of the deformation process from a sparse grid collocation of level 7 with 1274 sample points. These results were compared to those obtained with Monte Carlo using 6000 samples in Fig. 27.

8. Conclusions

The effect of uncertain initial geometry and texture on the final macroscale properties of the product of a multiscale deformation process is investigated through examples. A reduced-order representation of the random field representing texture is obtained using a bi-orthogonal Karhunen–Loève expansion. This reduced-order model introduces a new framework that makes the otherwise intractable task of quantifying the effect of random initial texture in a multiscale problem feasible. Many unresolved issues remain to be addressed including the selection of the dimensionality of the random space when no prior knowledge is available, simultaneously considering uncertainty sources on multiple scales (e.g. macroscale and mesoscale) and other.

Acknowledgements

The senior author (NZ) acknowledges support from the Computational Mathematics program of AFOSR (Grant F49620-00-1-0373), the Materials Design and Surface Engineering program of the NSF (Award CMMI-0757824), the Mechanical Behavior of Materials program Army Research Office (proposal to Cornell University No. W911NF0710519) and an OSD/AFOSR MURI09 award to Cornell University on uncertainty quantification.

References

[1] V. Sundararaghavan, N. Zabaras, Int. J. Plast. 24 (2008) 1581–1605.
[2] V. Sundararaghavan, N. Zabaras, Int. J. Plast. 22 (2006) 1799–1824.
[3] S. Ganapathysubramanian, N. Zabaras, Comput. Methods Appl. Mech. Eng. 193 (2004) 5017–5034.
[4] S. Acharjee, N. Zabaras, Comput. Struct. 85 (5-6) (2007) 244–254.
[5] R.G. Ghanem, P.D. Spanos, Stochastic Finite Elements: A Spectral Approach, Dover Publications, 1991.
[6] D. Xiu, J.S. Hesthaven, SIAM J. Sci. Comput. 27 (2005) 1118–1139.
[7] X. Ma, N. Zabaras, J. Comput. Phys. 228 (2009) 3084–3113.
[8] S.K. Sachdeva, P.B. Nair, A.J. Keane, Probab. Eng. Mech. 21 (2006) 182–192.
[9] D. Venturi, X. Wan, G.M. Karniadakis, J. Fluid Mech. 606 (2008) 339–367.
[10] S. Acharjee, N. Zabaras, Int. J. Numer. Methods Eng. 66 (12) (2006) 1934–1954.
[11] D. Alireza, R. Ghanem, J. Red-Horse, Comput. Methods Appl. Mech. Eng. 196 (2007) 3951–3966.
[12] B. Kouchmeshky, N. Zabaras, Comput. Mater. Sci. 47 (2) (2009) 342–352.
[13] B. Ganapathysubramanian, N. Zabaras, Comput. Methods Appl. Mech. Eng. 197 (2008) 3560–3573.
[14] L. Anand, M. Kothari, J. Mech. Phys. Solids 44 (1996) 525–558.
[15] A. Heinz, P. Neumann, Acta Crystallogr. A47 (1991) 780–789.
[16] A. Kumar, P.R. Dawson, Comput. Methods Appl. Mech. Eng. 130 (1996).
[17] H.J. Bunge, Texture Analysis in Materials Science, Butterworth, 1983.
[18] U.F. Kocks, C.N. Tomé, H.R. Wenk, Texture and Anisotropy – Preferred Orientations in Polycrystals and Their Effect on Materials Properties, Cambridge University Press, Cambridge, 2000.
[19] A. Kumar, P.R. Dawson, Comput. Mech. 17 (1995) 10–25.
[20] M. Rosenblatt, Ann. Math. Stat. 23 (1952) 470–472.
[21] I. Babuska, F. Nobile, R. Tempone, A Stochastic Collocation Method for Elliptic Partial Differential Equations with Random Input Data. ICES Report 2005, pp. 05–47.